Developmental Cell
Article

A Mechanical Jack-like Mechanism Drives Spontaneous Fracture Healing in Neonatal Mice

Chagai Rot,[1] Tomer Stern,[1] Ronen Blecher,[1] Ben Friesem,[1] and Elazar Zelzer[1,*]
[1]Department of Molecular Genetics, Weizmann Institute of Science, P.O. Box 26, Rehovot 76100, Israel
*Correspondence: eli.zelzer@weizmann.ac.il
http://dx.doi.org/10.1016/j.devcel.2014.08.026

SUMMARY

Treatment of fractured bones involves correction of displacement or angulation, known as reduction. However, angulated long-bone fractures in infants often heal and regain proper morphology spontaneously, without reduction. To study the mechanism underlying spontaneous regeneration of fractured bones, we left humeral fractures induced in newborn mice unstabilized, and rapid realignment of initially angulated bones was seen. This realignment was surprisingly not mediated by bone remodeling, but instead involved substantial movement of the two fragments prior to callus ossification. Analysis of gene expression profiles, cell proliferation, and bone growth revealed the formation of a functional, bidirectional growth plate at the concave side of the fracture. This growth plate acts like a mechanical jack, generating opposing forces that straighten the two fragments. Finally, we show that muscle force is important in this process, as blocking muscle contraction disrupts growth plate formation, leading to premature callus ossification and failed reduction.

INTRODUCTION

In vertebrates, the bone is one of a few organs that possess regenerative capabilities. There are two main challenges during the regeneration of a fractured bone. The first is to realign the bone, i.e., to correct displacement or angulation between the fragments of the fractured bone. In orthopedic medicine, this stage of treatment is termed reduction (Brorson, 2009; Court-Brown, 2010; Sarmiento et al., 1977). The second challenge is to unite the two fragments without scar tissue in order to restore the integrity and biomechanical quality of the bone (Giannoudis et al., 2007).

The importance of reduction to fracture healing and bone regeneration is well appreciated. Orthopedic literature establishes that reduction accelerates and improves the union process (Court-Brown, 2010). Nonetheless, it is common in human infants that substantially angulated fractures heal and bone morphology is restored without reduction (Caviglia et al., 2005; Husain et al., 2008). A possible and intriguing explanation for this phenomenon is that during infancy there is a natural mechanism that facilitates spontaneous realignment. Nevertheless, while the cellular, molecular, and mechanical factors that regulate fracture union have been extensively studied (Ai-Aql et al., 2008; Bolander, 1992; Cho et al., 2002; Dimitriou et al., 2005; Schindeler et al., 2008), a mechanism of natural reduction has not been described yet.

Past studies have characterized the various stages of the fracture healing process. The first is hematoma formation around the fracture site. Next, angiogenesis commences, followed by formation of soft, fibrocartilaginous callus. During the subsequent stages, the soft callus undergoes chondrogenesis and osteogenesis as cartilage is mineralized and replaced by hard, ossified callus. In the last stage, compact bone is formed by remodeling, and the bone's morphology is restored through modeling, which is bone resorption at the convexity and mineral deposition at the concavity (Einhorn, 1998; Gerstenfeld et al., 2003; Shapiro, 2008; Wilkins, 2005).

The ossification of soft callus bares similarities to the process of endochondral ossification during skeletogenesis (Ferguson et al., 1999; Gerstenfeld et al., 2003; Vortkamp et al., 1998). In this process, longitudinal bone growth is mediated by the growth plate, which is located at the two ends of the forming bone. The growth plate is composed of hierarchical layers of chondrocytes that undergo well-defined and highly controlled stages of proliferation and differentiation to hypotrophy (Karsenty and Wagner, 2002; Kronenberg, 2003; Olsen et al., 2000), which result in elongation. Concurrently, the cartilaginous template is replaced by ossified tissue.

Interestingly, another type of growth plate known as synchondrosis is located between the bones of the skull base. The synchondroses exhibit a remarkably organized structure, as each consists of two mirror-image growth plates facing opposite directions. These growth plates are fed by a shared resting zone located between them. The formation of double layers of prehypertrophic and hypertrophic chondrocytes drives growth in opposite directions, leading to expansion of the skull volume (Roberts and Blackwood, 1983; Young et al., 2006).

The growth plate mediates growth against substantial forces exerted by the musculature and by body weight. This suggests that the growth plate must also be able to generate considerable forces. Indeed, studies in various animal models as well as in humans suggest that the different growth plates can generate forces that range from the equivalent of 40% to 200% of body weight (Bylski-Austrow et al., 2001; Gelbke, 1951; Sijbrandij, 1963; Strobino et al., 1956; Wilson-MacDonald et al., 1990).

Although it is well known that during fracture healing the callus undergoes chondrogenesis and then ossification, this process has not been associated with bone realignment. In this work, we demonstrate that growth by endochondral ossification plays a central role in a mechanism whereby fractured bones regain

their morphology. We show that a bidirectional growth plate that promotes bone growth forms at the concave side of the fracture site. The bone growth generates force that drives the movement of the two bone fragments until alignment is achieved. Finally, we demonstrate that this ''mechanical jack''-like mechanism is regulated by muscle contraction.

RESULTS

Fractured Bones Realign in Neonate Mice

Little is known about the mechanism that underlies the ability of neonate bones with angulated fractures to regenerate and restore proper morphology. To gain insight into this mechanism, we produced mid-diaphyseal fractures with severe angulation of 20–80 degrees in humeri of postnatal day (P) 0 mice. To examine spontaneous morphological regeneration, fractured limbs were not stabilized, and movement of the mice was not restricted. In vivo micro computed tomography (micro-CT) scans were performed at P5 and P28 (Figure 1A), and realignment was examined in both the sagittal and coronal planes. As seen in Figures 1B and 1C, fractured humeri quickly regained their typical morphology. In most cases, angulations of up to 40° were completely realigned, whereas in more severely angulated bones (60°–80°), the angulation was markedly reduced to less than 20°. These results strongly imply that in neonate mice there is a robust mechanism for rapid morphological regeneration of fractured bones. The results also provided us with an excellent model system with which to study this mechanism.

Angulated Bones Realign by Movement of the Fracture Fragments

To uncover the mechanism that underlies natural reduction of fractured bones in newborn mice, we first sought to recover the morphological sequence that the fractured humeri undergo during the initial stages of the realignment process. For that, we performed daily in vivo CT scans of the same bone from P5 until P12. CT images showed that during that period the angle between the fracture fragments decreased quickly and substantially (Figures 1D–1F).

The reduction in angulation has commonly been attributed to massive bone modeling, which is a process that shapes ossified tissue through coordinated mineral deposition and resorption (Murray et al., 1996; Wilkins, 2005). However, the observed rapid day-to-day changes occurred prior to callus ossification (Figures 1G and 1G'). This suggested that the naturally occurring reduction was accomplished by another mechanism, such as movement of the fracture fragments. To clarify this issue, we analyzed temporal preservation of mineralized areas during realignment by labeling newly deposited bone surface with different fluorochromes. Since bone modeling involves substantial mineral resorption, temporal preservation of fluorochrome-labeled areas would rule out the possibility of realignment by modeling and would strongly support the fragment movement hypothesis. Following fracture induction at P0, humeri were labeled with calcein (green) at P3 or P6 and with alizarin (red) at P5 or P8. At P6 or P9, when a decrease in angulation was already evident (Figure 1G' and Figure S1A' available online), the bones were examined histologically. Results showed that calcein-labeled regions of the endosteum were maintained in both fracture fragments (Figures 1G'' and S1A''), as in the intact contralateral control bone (Figures 1H', 1H'', and S1B''). These results demonstrate that the decrease in angulation of fractured bones is a consequence of fragment movement rather than of modeling. This finding challenges the traditional view of fracture healing and implies that a previously unknown mechanism of natural reduction participates in the regeneration process.

Asymmetric Callus Formation at the Fracture Site

Our finding that natural reduction of fractured bones involves movement of the two fragments raised the question of the source of the force that drives this movement. The formation of callus that stabilizes the fracture site is a hallmark of fracture healing and, as such, an immediate suspect. We therefore analyzed callus formation during fragment movement. Histological analysis of the fracture site showed hematoma at P3 (Figures 2A–2A''). By P5, extensive formation of soft, fibrocartilaginous callus was seen around the edges of the two fragments (Figure 2B). Notably, at the concave side, cells that appeared as prechondrocytes were observed; at that stage, there was no sign of bone formation (Figures 2B' and 2B''). At P7, chondrocytes at various differentiation states where observed at the concave side, including cells that appeared hypertrophic. Concurrently, the cells at the convex side of the fracture site maintained a fibrocartilaginous appearance (Figures 2C–2C''). By P9, while asymmetric chondrogenesis in the callus continued, both fragment ends contained new trabecular bone. The process of bone formation progressed from the edge of the fragments toward the space between them (Figures 2D–2D'').

These results show that in unstabilized fractures, the callus undergoes asymmetric cartilage formation, which might be involved in the natural reduction mechanism.

Fracture Callus Operates as a Bidirectional Growth Plate during Natural Reduction

Our finding of asymmetric chondrogenesis in the callus of unstabilized fractures led us to hypothesize that during natural reduction, the callus functions as an active growth plate to promote bone formation, which in turn generates the force that drives the movement of the two fracture fragments. To test this hypothesis, we analyzed the expression patterns of collagen type II (*Col2a1*), collagen type X (*Col10a1*), Indian hedgehog (*Ihh*), and Patched (*Ptc*), which are markers for different stages of chondrocyte differentiation in the growth plate. We performed the analysis at two stages during the alignment process: first at P4, when formation of soft fibrocartilaginous callus begins, and then at a stage (P8), when the realignment process was at its peak, i.e., after a large movement has occurred but before full straightening was achieved (Figures S2A and S2B). As expected, results showed that the expression of chondrogenic markers was much more prominent at the concave side of the fracture, relative to the opposite side (Figures 3A–3B'). These results supported the possibility that a growth plate has formed at the concave side of the fracture site.

Another intriguing observation was that at the concave side, the expression domains observed at the proximal edge of the callus were also observed at the distal edge (Figure 3B'). The mirror expression of chondrogenic markers suggests that unlike in the epiphyseal growth plate, in fracture callus, a bidirectional

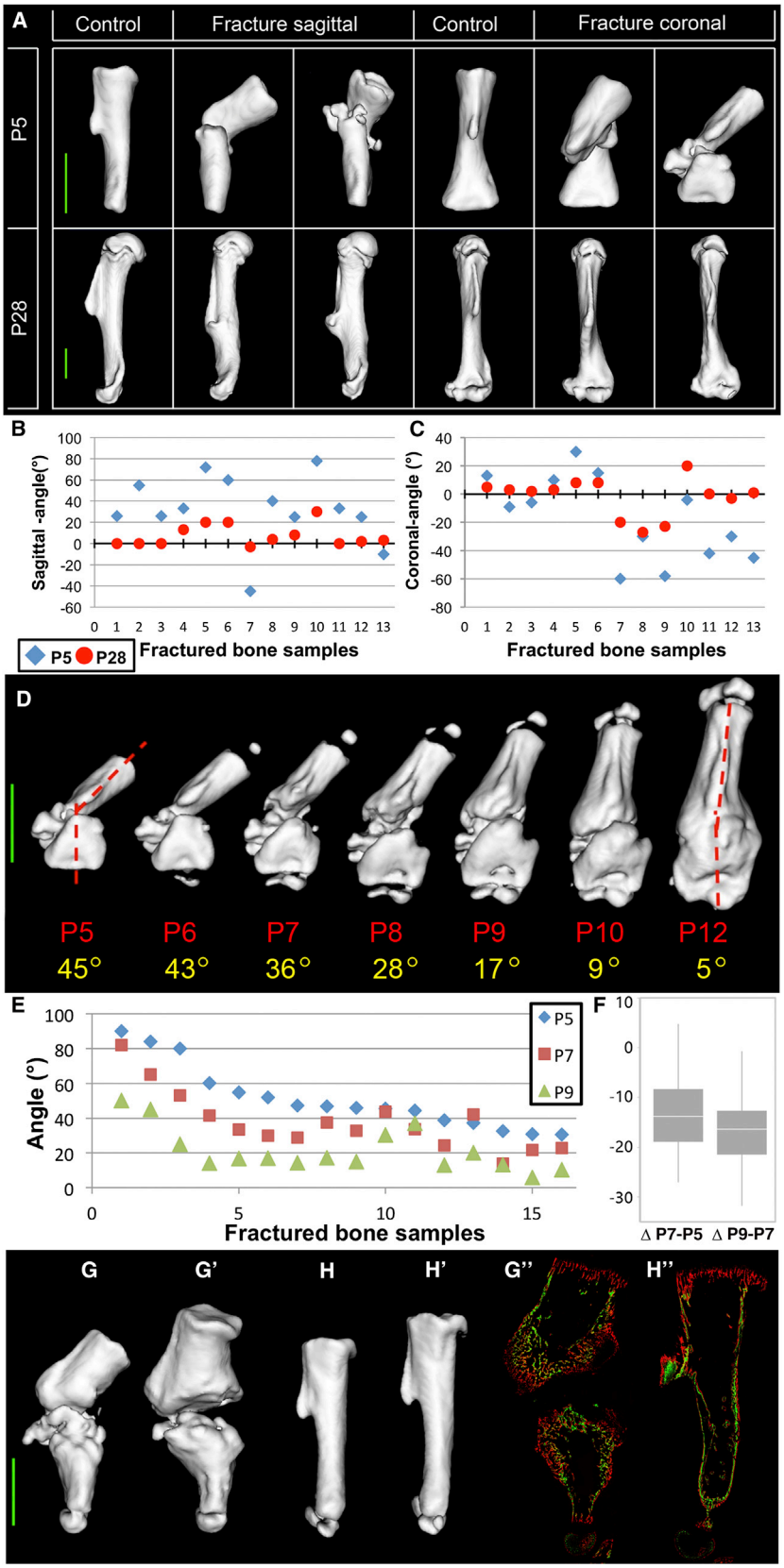

Figure 1. Natural Reduction of Fractured Humeri Is Mediated by Fragment Movement

(A) Sagittal plane (left) or coronal plane (right) views of 3D reconstructions from in vivo CT images of four fractured humeri from different mice and an intact control bone at P5 (top) and at P28 (bottom).

(B and C) Scatter plots showing the angle between the two fragments of all fractured humeri (n = 13) as measured at P5 (blue diamond) and at P28 (red circle) either in the sagittal plane (B), where positive values represent caudal shift and negative values represent cranial shift, or in the coronal plane (C), where positive/negative values relate to medial or lateral shift, respectively.

(D) Daily sequence of 3D in vivo micro-CT images showing dramatic and rapid decrease in angulation between P5 and P12.

(E) Scatter plots showing the angle between the two fragments of all fractured humeri (n = 16) as measured at P5 (blue diamond), P7 (red box), and P9 (green triangle). Samples with an initial angle higher than 30 degrees are ordered from left to right by severity of angulations at P5.

(F) Box plot of angulation reduction from P5 to P7 and from P7 to P9.

(G–H'') Fractured left humeri and corresponding intact right humeri were labeled at P6 with calcein (green) and scanned at P7 (G and H), and then labeled at P8 with alizarin (red) and scanned at P9 (G' and H'), followed by histological analysis (G'' and H''). In both fractured and control bones calcein-labeled regions of the endosteum were maintained, negating the possibility of significant bone modeling. Scale bars, 2 mm.

See also Figure S1.

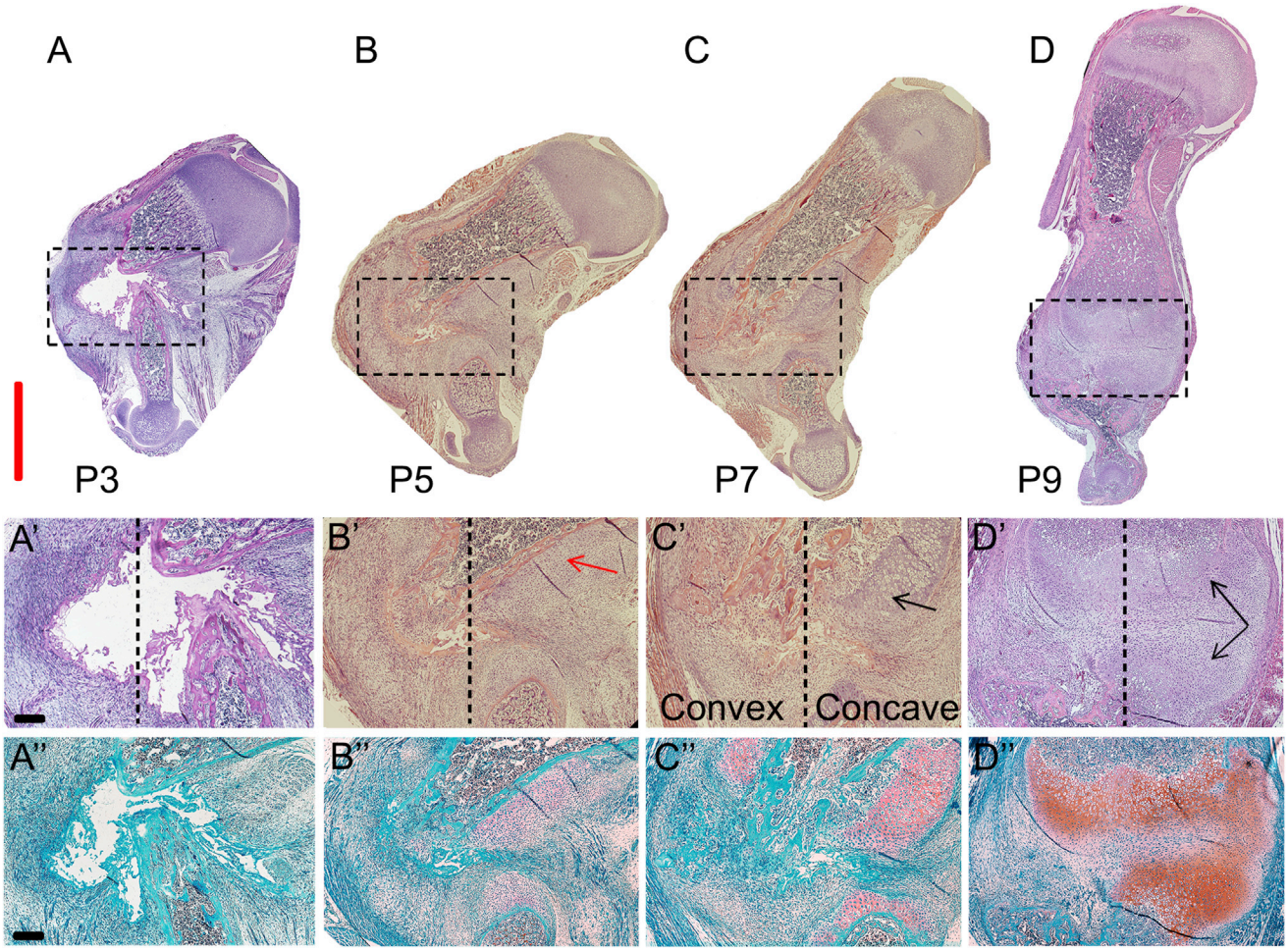

Figure 2. Asymmetric Callus Formation at the Fracture Site

(A–D) H&E and Safranin O/Fast Green staining of sections through the fracture site during the healing process (P3–P9). Scale bar, 2 mm.

(A'–D') Magnifications of the boxed areas in the upper panel. Dashed lines separate between the concave side (on the right) and convex side. Red arrow indicates cells appearing as chondrocytes, and black arrows indicate cells appearing as hypertrophic chondrocytes.

(A''–D'') As indicted by Safranin O staining (pink-to-red colors), as the healing process progresses the soft callus is increasingly composed of cartilage. Scale bar, 200 μm.

growth plate is formed. A presumably similar structure is seen in the synchondroses, which are located between the bones of the skull base (Figure S2C) and create movement in opposite directions to expand the skull volume. To verify this assumption, we compared the expression of growth plate markers in the synchondrosis to their expression in the presumable callus growth plate. As can be seen in Figure 3C, expression patterns were comparable, thus supporting our hypothesis that the callus growth plate is bidirectional and therefore able to generate force in opposite directions, as in the synchondrosis (Figures 3B'' and 3C').

Next, we examined another hallmark of an active growth plate, namely chondrocyte proliferation, in the callus by BrdU assay. Results showed high proliferation activity in the callus (Figure 3D), with significantly higher levels at the concave side relative to the convex side (Figure 3E). Finally, to establish that a functional bidirectional growth plate is formed at the concave side of the fracture site, it was necessary to demonstrate local bone formation. For quantitative assessment of bone formation, in vivo CT images of bone fragments at P7 were superimposed on images of the same fragments at P9 (Figures 3F–3F''). The superimposed images revealed extensive bone growth, which was most prominent at the presumptive location of the bidirectional growth plate (Figure 3G).

Taken together, these results demonstrate that an active bidirectional growth plate is formed at the concave side of the callus to mediate bone growth. This finding strongly supports our hypothesis that bone growth by the bidirectional growth plate generates the force required for the movement of the two fracture fragments during reduction, similar to a "mechanical jack" mechanism.

Callus Ossification Begins after Most of the Angulation Has Been Reduced

A critical element in our model is the timing of termination of growth plate activity and ossification of the fracture site. As

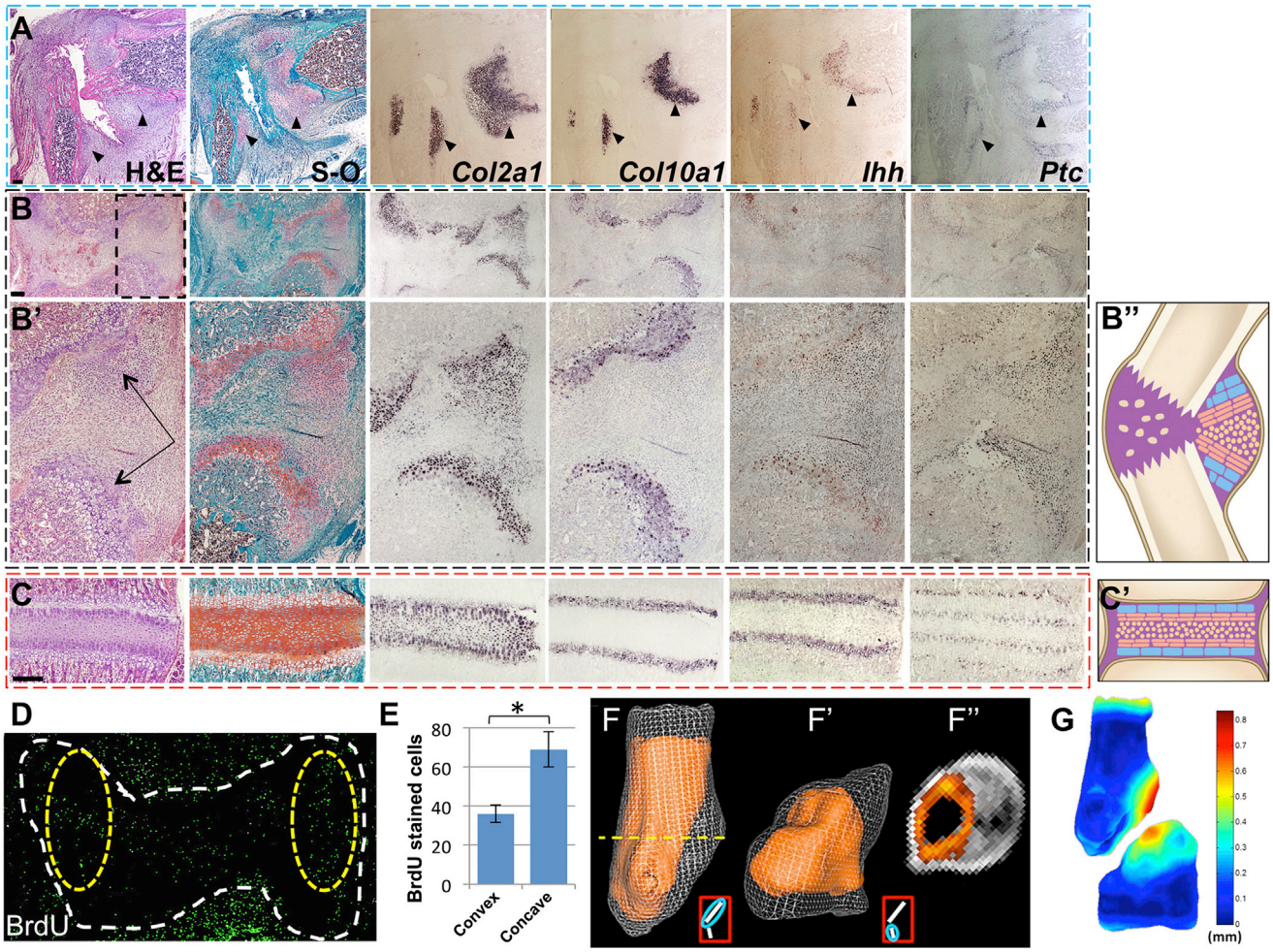

Figure 3. Fracture Callus Operates as an Active Bidirectional Growth Plate

(A and B) Histological staining with H&E and Safranin O/Fast Green of the fracture site and in situ hybridization for growth plate markers *Col2a1*, *Col10a1*, *Ihh*, and *Ptc* at P4 and P8, respectively.

(B') Magnifications of the concave side (dashed rectangle in B). Mirror expression of growth plate markers (arrows; arrowheads in A) indicates the formation of a bidirectional growth plate.

(B'') Schematic illustration of the mechanical jack-like effect of fracture callus operating as a bidirectional growth plate.

(C) Histological, gene expression, and proliferation analyses show comparable patterns in the skull base spheno-occipital synchondrosis. Scale bar, 200 μm.

(C') Schematic of a synchondrosis, where two mirror-image growth plates face opposite directions.

(D) BrdU staining at P8. White dashed line demarcates the callus area, and yellow ellipses demarcate convex (left) and concave sides.

(E) Comparison of BrdU-stained cell numbers shows significantly higher proliferation at the concave side of the fracture, relative to the convex side. Significant differences ($p \leq 0.05$) are marked with asterisks; data are presented as mean ± SEM.

(F and F') Triangulated grid of the external surfaces of the two fragments of a P9 bone (white) superimposed on the corresponding isosurfaces at P7 (orange) shows callus growth during this interval.

(F'') Transverse slice from the superimposed proximal bone fragments at the location marked by a dotted yellow line in F.

(G) The surface of the bone was color-coded to indicate level of bone formation between P7 to P9; the color bar indicates growth in millimeters. Extensive bone growth is seen exclusively at the concave side of the fracture.

See also Figure S2.

long as the bone is not properly aligned, growth-plate-mediated fragment movement must continue. In addition, delay in callus ossification is necessary to maintain flexibility of the fracture area in order to allow movement. However, once alignment is achieved, the growth plate must undergo rapid ossification to stabilize the bone at the correct position. To test these assumptions, CT images were analyzed to determine the time point at which fracture callus undergoes ossification and compare it with the sequence of reduction in angulation.

CT images of fractured bones were taken every other day from P5 (Figure 4A) until P17 and at P28. At P9, when substantial straightening has already occurred (Figure 4B), the space between the two fragments was still unmineralized (Figure 4B'). Only between P11 and P15 we observed ossified callus in this domain (Figures 4C and 4C'). Histological examination and

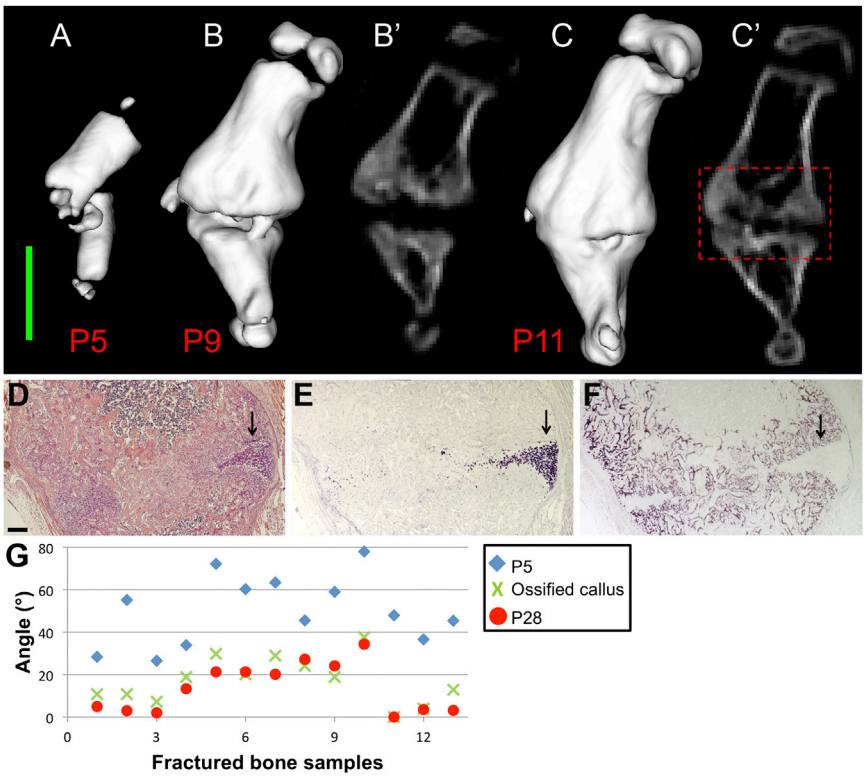

Figure 4. Callus Ossification Progresses after Most of the Realignment Has Occurred

(A–C) 3D in vivo CT images of a fractured humerus at P5 (A), P9 (B), and P11 (C).

(B' and C') 2D in vivo CT images of the same bone at P9 and P11, respectively. Scale bar, 2 mm.

(D–F) Magnifications of the concave side of the fracture, demarcated by a red dashed box in (C'). The presence of chondrocytes (indicated by black arrows) is demonstrated by H&E staining (D) and by in situ hybridization for *Col10a1* (E). The progression of the mineralization process from the convex toward the concave side is shown by the osteoblastic marker *Bsp* (F). Scale bar, 200 μm.

(G) Scatter plot showing the angle between the two fragments of all fractured humeri (n = 13), as measured at P5 (blue diamond), during callus ossification (P11–P15, green X) and at P28 (red circle).

expression analysis of chondrocyte marker *Col10a1* and osteoblast marker bone sialoprotein (*Bsp*) supported the CT results, demonstrating callus ossification through the center of the fracture site (Figures 4D–4F). Next, we examined changes in angulation during this period. As seen in Figure 4G, in all examined samples (n = 13), most of the angulation was reduced prior to ossification, whereas from the ossification stage until P28 there was relatively little change. These results indicate the major contribution of natural reduction to fractured bone regeneration. Moreover, they imply the importance of maintaining the callus unossified, as premature ossification would restrict movement-induced natural reduction.

Muscle Contraction Temporally Regulates Callus Ossification

Having established the main characteristics of the natural reduction mechanism, we proceeded to explore how it is controlled. As mentioned, temporal control of callus ossification is essential to prevent premature loss of the bidirectional growth plate activity. It is generally accepted that during fracture healing, instability and motion at the site of the fracture lead to the formation of cartilaginous callus, whereas rigid stabilization leads to reduced cartilage formation and direct repair by intramembranous ossification (Thompson et al., 2002). Skeletogenesis and embryonic physeal growth require viable contracting skeletal muscles (Germiller and Goldstein, 1997; Shwartz et al., 2012, 2013). Therefore, we hypothesized that muscle forces play a role in the control of growth plate formation and activity in the callus. To test this assumption, we removed the contractile force of muscles from the fracture area during regeneration by injecting botulinum toxin type A (Botox) at P5 into the muscles around the fracture site. Botulinum toxin inhibits acetylcholine release by preventing vesicles from anchoring to the neuromuscular membrane, thereby paralyzing the muscle (Huang et al., 2000). Comparative in vivo CT imaging of P5 to P17 mice with a fractured humerus (n = 5) revealed that in the absence of muscle activity, natural reduction failed (Figure 5A). To quantify the effect of muscle contraction on natural reduction, the level of angulation was measured in bones of Botox-treated mice (n = 13). The results showed that unlike in the control, Botox administration at P5 leads to reduction arrest by P7 (Figures 5B–5E).

To gain histological and molecular understanding of the failure in natural reduction in Botox-treated mice, we compared callus differentiation state at P7 and P9 between control and treated mice. Expression analysis of SRY box containing gene 9 (*Sox9*), *Col2a1*, and *Col10a1* revealed that the absence of muscle contraction led to symmetric chondrogenesis and loss of the bidirectional growth plate organization (Figures 6A–6G'). Instead, accelerated osteogenesis was observed in the central region of the fracture (Figure 6D'), evident also by the expression of collagen type I (*Col1a1*) (Figure 6H'). Finally, BrdU staining showed a decrease in cell proliferation relative to the control, without noticeable differences between the two sides of the fracture site (Figures 6I and 6J). To rule out the possibility that reduced proliferation of callus cells was a consequence of a direct Botox effect, we examined proliferation in two other tissues near the fracture site, namely bone marrow cells and muscle cells. Results showed no effect on marrow cells and a moderate effect on muscle cell proliferation (Figure S3), unlike the intense effect observed in callus cells.

Together, these results imply that in the absence of muscle contraction the callus fails to organize and act as a growth plate and undergoes early ossification; consequently, the fracture remains angulated (Figures 6K and 6L). These findings strongly imply that muscle contraction controls the establishment of the bidirectional growth plate and thereby the reduction process during bone regeneration.

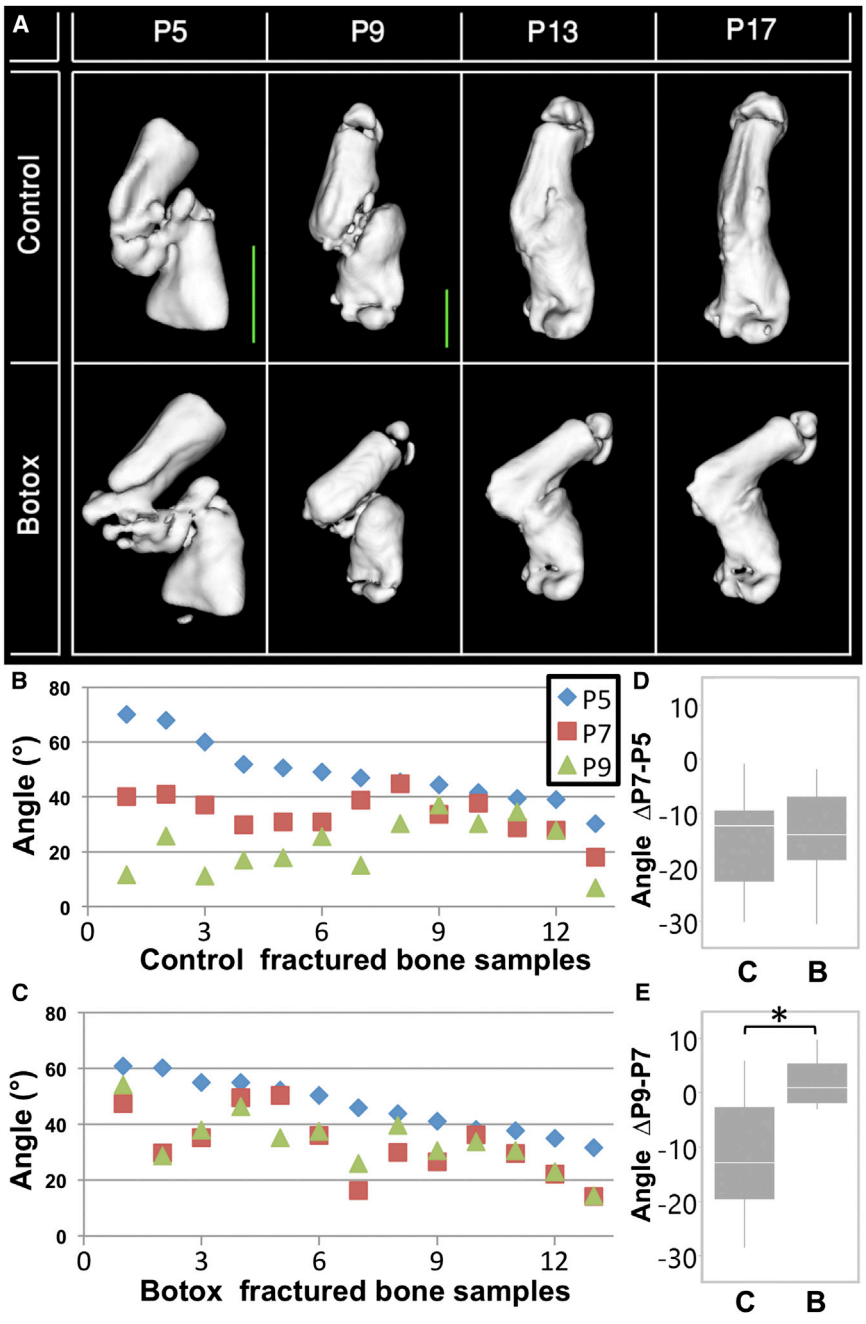

Figure 5. Natural Reduction Fails in the Absence of Muscle Contraction

(A) 3D reconstructions of in vivo CT images of fractured humeri from mice injected with Botox to paralyze the triceps brachii muscle (bottom row) and from control mice injected with PBS (top row). Scale bars, 2 μm.

(B and C) Scatter plots showing the angle between the two fragments of all fractured humeri in the control (B, n = 13) and Botox-treated groups (C, n = 13) as measured at P5 (blue diamond), P7 (red box), and P9 (green triangle). Samples with an initial angle higher than 30 degrees are ordered from left to right by severity of angulations at P5. There were no statistically significant differences between the groups in angulation at P5.

(D and E) Box plots of angulation reduction from P5 to P7 (D) and from P7 to P9 (E) in Botox-treated (B) and control (P) groups. A statistically significant difference ($p < 0.001$) between the groups was measured during the second interval (marked by an asterisk), but not in the first.

DISCUSSION

The importance of morphology to the function of bones is well appreciated. It is therefore reasonable to assume that mechanisms of bone regeneration should include morphogenetic capabilities. Indeed, several lines of evidence have suggested the existence of a robust mechanism for morphogenetic regeneration. At the beginning of the 20th century, studies of skeletons of different kinds of primates were conducted. Those studies revealed a relatively high rate of animals (up to 30%) that exhibited evidence of healed fractures (Bramblett, 1967; Duckworth, 1911; Schultz, 1939, 1944). Interestingly, the fractures were suggested to have occurred in young apes, and in most cases, the bones healed with relatively little deformity (Bulstrode, 1990). This suggests that during evolution vertebrates have acquired a mechanism that realigns fractured bones (Currey, 2002). Another strong indication for the existence of a morphological regeneration mechanism is the naturally occurring reduction during the healing of humeral fractures in human infants, during which severely angulated bones restore normal morphology (Caviglia et al., 2005; Husain et al., 2008).

To date, there are two morphogenetic processes that are known to be involved in bone realignment. Bone modeling, also known as bone drift, mostly affects the bone shaft at the fracture site. In accordance with Wolff's law (Wolff, 1892), it involves bone resorption at the convexity and mineral deposition at the concavity (Murray et al., 1996; Wilkins, 2005). The second process is reorientation of the growth plates, which leads to asymmetric epiphyseal growth and thereby to bone alignment (Karaharju et al., 1976; Wallace and Hoffman, 1992). Although the contribution of these mechanisms is unquestionable, it is also limited. Modeling starts to act only after the fracture callus has undergone ossification, implying that it cannot expedite the union process. Realignment by asymmetric epiphyseal growth depends on substantial elongation of the bone and is therefore a slow process.

Here, we present a mechanism of natural reduction that acts rapidly and efficiently prior to callus ossification and does not depend on epiphyseal growth. Natural reduction relies on movement of the two parts of the fractured bone toward alignment.

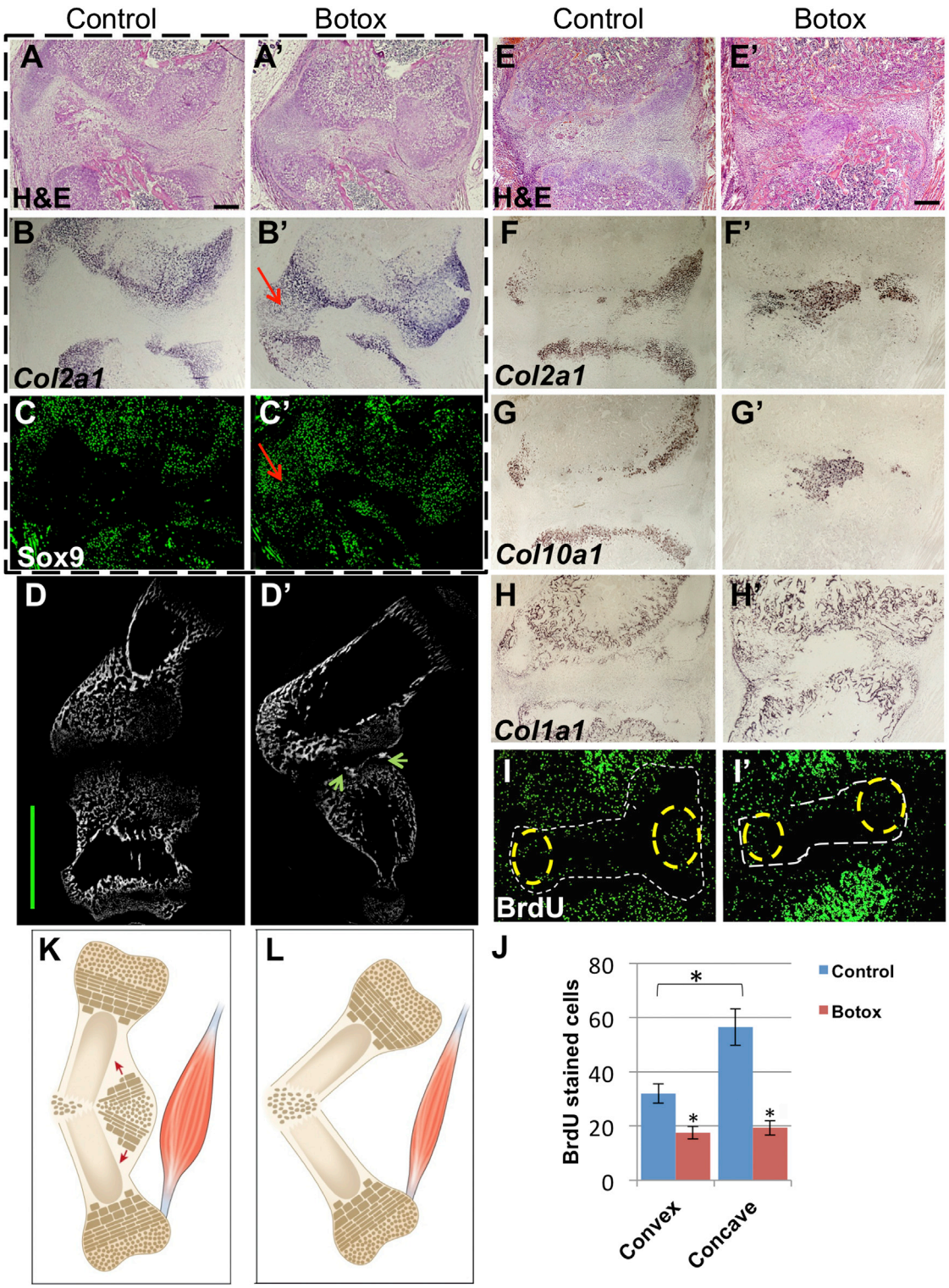

Figure 6. Muscle Contraction Regulates Bidirectional Growth Plate Formation and Callus Ossification

(A and A') H&E-stained histological sections of fracture callus at P7 in control (A) and Botox-treated (A') mice show symmetric chondrocyte distribution through the fracture site in treated mice.

(B–C') In situ hybridization for the chondrocyte marker *Col2a1* (B and B') and immunostaining for the prechondrogenic marker SOX9 (C and C') at P7 demonstrate symmetric callus formation through the fracture site in treated but not in control mice. Red arrows indicate callus differentiation at the convex side.

(legend continued on next page)

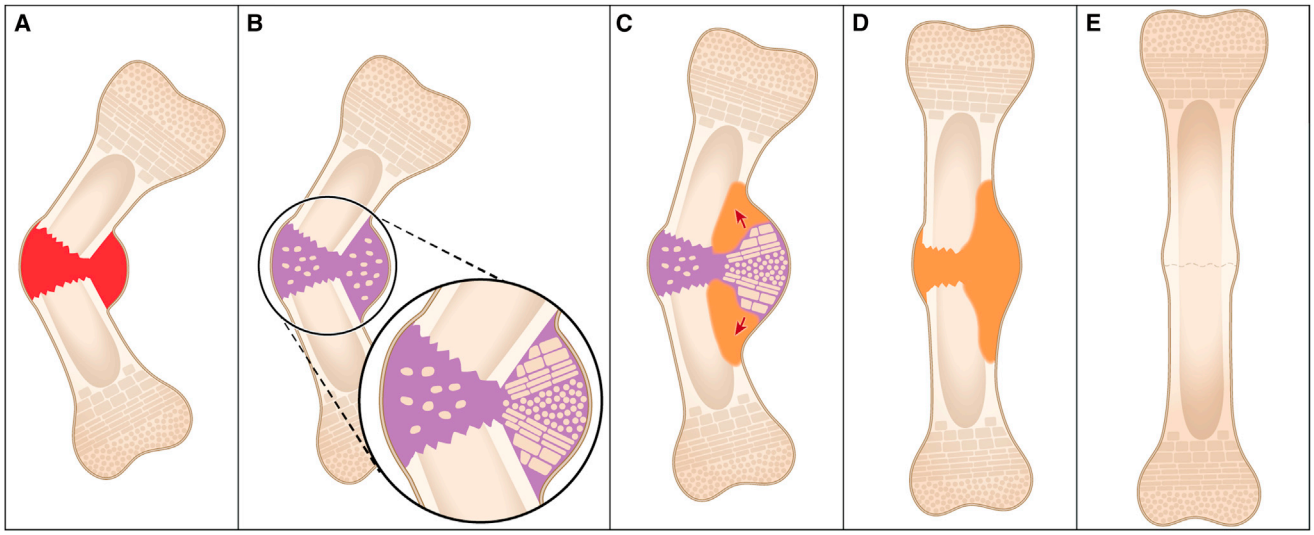

Figure 7. The Concept of Natural Reduction Expands the Traditional Four-Stage Classification of Fracture Healing

(A) Healing begins with hematoma and inflammation at the fracture site.

(B) Soft callus (purple) is formed, which we show to organize as a bidirectional growth plate at the concave side of the fracture site.

(C) The two growth plates drive growth in opposite directions. The result is a jack-like mechanical effect that moves the fragments toward straightening (red arrows).

(D) Ossification produces hard callus (orange).

(E) The shape of the bone is fine-tuned by remodeling.

The evolutionary advantage of this strategy is that realignment is fast and therefore conditions for bony union are optimized (Sarmiento et al., 1977), much like the rationale behind orthopedic reduction. Our results clearly demonstrate that most of the realignment is achieved by fragment movement, whereas modeling and growth plate reorientation have only minute contributions. The finding of this program implies an expansion of the four-stage classification of bone repair introduced by John Hunter in 1768 (Hunter, 1837). We suggest that for young animals, a stage of natural reduction be added between the second stage of soft callus formation and the third stage of hard callus formation (Figure 7).

The similarities between fracture healing processes and endochondral ossification were previously recognized (Ferguson et al., 1999; Gerstenfeld et al., 2003; Vortkamp et al., 1998). However, it has been assumed that unlike in development, during fracture healing, cartilaginous callus only serves as a template for ossification and is not involved in promoting bone growth. Now our work demonstrates that all of the characteristics of an active growth plate exist in the callus at the concave side of the fracture site, including gene expression profiles, cell proliferation, and bone growth. We therefore argue that the growth plate in the callus serves not only for intermediate stabilization, but also to actively promote bone reduction. However, unlike the epiphyseal growth plates and similar to the synchondroses that mediate cranial base expansion, the bidirectional growth plate at the fracture site drives growth in opposite directions. This generates force that moves the fragments toward straightening in a mechanical jack-like effect. The formation of a bidirectional growth plate at the fracture site raises several interesting questions. The first regards the signals that control the formation of a growth plate. Surprisingly, little is known about these signals not only during fracture healing but during development as well. Another

(D and D') Higher-resolution (5 μm), postsacrifice 2D micro-CT images of control (D) and Botox-treated (D') fractured bones at P9. Unlike in control mice, mineralized fragments are seen in the callus of treated mice (indicated by green arrows). Scale bar, 2 mm.

(E and E') H&E-stained histological sections of fracture callus at P9 from control (E) and Botox-treated (E') mice show in the latter reduced and less organized cartilage and patches of apparently mineralized tissue.

(F–H) In situ hybridization for growth plate markers *Col2a1* and *Col10a1* and osteoblast marker *Col1a1*. There are far less differentiated (*Col2a1*-positive, F') and hypertrophic (*Col10a1*-positive, G') chondrocytes at the two bone-callus interfaces in Botox-treated mice relative to control mice (F and G, respectively); in addition, the distinctive spatial organization is lost. Expression patterns of *Col1a1* indicate more osteoblasts in the callus of treated mice (H'), as compared with control mice (H).

(I and I') BrdU immunostaining illustrates a striking difference in cell proliferation at the concave side between control (I) and treated mice (I'). Scale bar, 200 μm.

(J) Comparison of BrdU-stained cell count between the concave and convex sides of the fracture in control and Botox-treated mice. Significant differences ($p \leq 0.05$) are marked with asterisks; data are presented as mean ± SEM.

(K) When the two growth plates induce growth in opposite directions, the resulting jack-like effect moves the fragments toward straightening (red arrows).

(L) In the absence of muscle contraction, the callus fails to organize and act as a growth plate and undergoes premature ossification; consequently, the bone remains deformed.

See also Figure S3.

interesting question relates to the regulation of the formation of different types of growth plates, namely epiphyseal or bidirectional. Finally, the signals that terminate the activity of the bidirectional growth plate at the fracture site are yet to be uncovered.

Mechanical forces exerted by muscles have been demonstrated by us and others to play a variety of important roles in skeletogenesis (Hall and Herring, 1990; Kahn et al., 2009; Nowlan et al., 2008; Sharir et al., 2011; Shwartz et al., 2012, 2013). Here, we demonstrate a role for muscle contraction in bone healing. Through a yet-unknown mechanism, the musculature regulates the formation and the activity of the bidirectional growth plate. This finding correlates well with previous works that demonstrated the involvement of movement in determining callus chondrogenesis (Giannoudis et al., 2007; Le et al., 2001). Moreover, finite element analysis of local strains and stresses at the fracture site suggested that compressive forces promote endochondral ossification, whereas tensile forces lead to fibrocartilage and connective tissue differentiation (Claes and Heigele, 1999). The latter report fits well with our findings since at the concave side, where compressive forces are high (Tencer 2010), chondrogenesis was seen to take place, whereas at the convex side, where tensile forces are high, we observed reduced chondrogenesis and cells that appeared as fibrocartilage.

To conclude, we present in this work a paradigm for fractured bone regeneration. We show that untreated angulated fractures undergo a realignment process that we term natural reduction. We provide evidence that a bidirectional growth plate is the cellular entity that generates the force required for this process. We then demonstrate the significance of muscle contraction in the temporal regulation of the bidirectional growth plate during natural reduction. Our findings underscore the robustness of bone regeneration mechanisms. From an evolutionary perspective, the mechanism we uncover increases the chances of vertebrates to survive traumatic injury. Our findings may also have implications for bone fracture treatment. For that to happen, several fundamental questions need to be addressed. These relate to the genetic program and signaling networks that control the establishment, activity, and termination of a growth plate in the fracture callus and to how the fractured bone ''knows'' its orientation.

EXPERIMENTAL PROCEDURES

Animals and Bone Fracture Induction

Imprinting control regions mice were purchased from Harlan Laboratories. Humeral fractures were induced at P0 by surgical incision through the middle area of the bone shaft (for more details, see Supplemental Experimental Procedures). All experiments were approved beforehand by the Institutional Animal Care and Use Committee of the Weizmann Institute.

The induction of fractures by incision was expected to produce high variation in fracture morphology and angulation. Therefore, in order to standardize the experimental process, mice with substantial initial displacement or with fractures located distantly from the mid-diaphysis were excluded from the study. Another issue that had to be addressed was the complexity of the 3D morphology of fracture callus. To simplify the analysis, only bones angulated mostly in one plane were included in the histological and gene expression analyses (Figures S4A and S4B). However, mice exhibiting more morphologically complex fractures (Figure S4C) were subsequently included in gross morphology analyses, such as assessments of angulation and reduction.

Computed Tomography Analyses

To visualize the process of bone healing, mice were anesthetized with isoflurane (2-chloro-2-(difluoromethoxy)-1,1,1-trifluoro-ethane) and scanned in vivo by micro-CT. Scans were performed with TomoScope 30S Duo scanner (CT Imaging) equipped with two source-detector systems. The operation voltage of both tubes was 40 kV. Integration time was 90 ms, and the isotropic resolution was 76 mm. Data were analyzed using the MicroView software (GE Healthcare, v.5.2.2). A Detailed description of ex vivo CT analysis is provided in Supplemental Experimental Procedures.

Histology, In Situ Hybridization, BrdU Assay, and Immunofluorescence Staining

For section preparation, see the Supplemental Experimental Procedures. Hematoxylin and eosin (H&E) and Safranin O/Fast Green staining was performed following standard protocols. In situ hybridization on paraffin sections was performed as described previously (Murtaugh et al., 1999; Riddle et al., 1993) using digoxigenin-labeled probes. All probes are available on request. For BrdU assay, which was performed as described previously (Blitz et al., 2009), mice were injected intraperitoneally with 100 mg/kg body weight of BrdU labeling reagent (Sigma) and sacrificed 2 hours later. For immunofluorescence staining for SOX9, primary anti-SOX9 antibody (1:200; AB5535; Millipore) was used.

Evaluation of Bone Deposition and Resorption

See the Supplemental Experimental Procedures.

Bone Registration and Appositional Growth Calculations

See the Supplemental Experimental Procedures.

Measurement of Fracture Angulation

To measure the angle between fracture fragments, the isosurface was first extracted to generate a 3D representation of the ossified bone. Next, the formed surface was manually repositioned and rotated to align the sagittal and coronal planes of the bone with the (x,z) and (y,z) planes of the image grid, respectively. Then the angle between proximal and distal fragments was measured manually in each plane, and the fracture angle was calculated using a mathematical equation. For further details, see Supplemental Experimental Procedures.

Muscle Paralysis by Botox

Mice were injected with botulinum toxin A (Botox, Allergan; 0.15 U, 10 μl final volume) into the left triceps muscle group every 2 days continuously. Control mice were given intramuscular injections of PBS. Botox-treated mice exhibited weight growth retardation, an observation consistent with a previous report (Thomopoulos et al., 2007).

Statistical Analysis

To assess the realignment of fractured bones, angulations at P5 and the reduction in angulations between P5 and P7 and between P7 and P9 were compared between the Botox treatment group (n = 13) and control group (n = 13) using Student's t test or unequal variance t test when prompted. To quantify the rate of cell proliferation, serial images of callus from the same sectors were collected, and BrdU-positive chondrocytes were counted in four control and four Botox-treated mice from two different litters. At least three sections were counted for each sample. Statistical significance was determined by Student's t test; p values of 0.05 or less were considered significant.

SUPPLEMENTAL INFORMATION

Supplemental Information includes Supplemental Experimental Procedures and four figures and can be found with this article online at http://dx.doi.org/10.1016/j.devcel.2014.08.026.

ACKNOWLEDGMENTS

We thank N. Konstantin for editorial assistance; Dr. Shaul Beyth from the Orthopedic Surgery Department, Hadassah University Hospital for discussions, ideas, and encouragement; Dr. Yoni Vortman from the Department of

Evolutionary and Environmental Biology, University of Haifa for assistance with the statistical analyses; and Genia Brodsky from the Graphic Design Department for her help with designing the graphic model. Special thanks are given to all members of the Zelzer laboratory for their advice and suggestions. This work was supported by a grant from the European Research Council (ERC) (#310098).

Received: May 19, 2014
Revised: July 22, 2014
Accepted: August 28, 2014
Published: October 27, 2014

REFERENCES

Ai-Aql, Z.S., Alagl, A.S., Graves, D.T., Gerstenfeld, L.C., and Einhorn, T.A. (2008). Molecular mechanisms controlling bone formation during fracture healing and distraction osteogenesis. J. Dent. Res. *87*, 107–118.

Blitz, E., Viukov, S., Sharir, A., Shwartz, Y., Galloway, J.L., Pryce, B.A., Johnson, R.L., Tabin, C.J., Schweitzer, R., and Zelzer, E. (2009). Bone ridge patterning during musculoskeletal assembly is mediated through SCX regulation of Bmp4 at the tendon-skeleton junction. Dev. Cell *17*, 861–873.

Bolander, M.E. (1992). Regulation of fracture repair by growth factors. Proc. Soc. Exp. Biol. Med. *200*, 165–170.

Bramblett, C.A. (1967). Pathology in the Darajani baboon. Am. J. Phys. Anthropol. *26*, 331–340.

Brorson, S. (2009). Management of fractures of the humerus in Ancient Egypt, Greece, and Rome: an historical review. Clin. Orthop. Relat. Res. *467*, 1907–1914.

Bulstrode, C. (1990). What happens to wild animals with broken bones. Iowa Orthop. J. *10*, 19.

Bylski-Austrow, D.I., Wall, E.J., Rupert, M.P., Roy, D.R., and Crawford, A.H. (2001). Growth plate forces in the adolescent human knee: a radiographic and mechanical study of epiphyseal staples. J. Pediatr. Orthop. *21*, 817–823.

Caviglia, H., Garrido, C.P., Palazzi, F.F., and Meana, N.V. (2005). Pediatric fractures of the humerus. Clin. Orthop. Relat. Res. (432), 49–56.

Cho, T.-J., Gerstenfeld, L.C., and Einhorn, T.A. (2002). Differential temporal expression of members of the transforming growth factor β superfamily during murine fracture healing. J. Bone Miner. Res. *17*, 513–520.

Claes, L.E., and Heigele, C.A. (1999). Magnitudes of local stress and strain along bony surfaces predict the course and type of fracture healing. J. Biomech. *32*, 255–266.

Court-Brown, C.M. (2010). Principles of nonoperative fracture treatment. In Rockwood and Green's Fractures in Adults, C.A. Rockwood, D.P. Green, and R.W. Bucholz, eds. (Philadelphia: Lippincott Williams & Wilkins).

Currey, J.D. (2002). Safety factors and scaling effects in bones. In Bones: Structure and MechanicsBones: Structure and Mechanics (Princeton: Princeton University Press), pp. 310–327.

Dimitriou, R., Tsiridis, E., and Giannoudis, P.V. (2005). Current concepts of molecular aspects of bone healing. Injury *36*, 1392–1404.

Duckworth, W. (1911). On the natural repair of fractures, as seen in the skeletons of anthropoid apes. J. Anat. Physiol. *46*, 81.

Einhorn, T.A. (1998). The cell and molecular biology of fracture healing. Clin. Orthop. Relat. Res. (355, Suppl), S7–S21.

Ferguson, C., Alpern, E., Miclau, T., and Helms, J.A. (1999). Does adult fracture repair recapitulate embryonic skeletal formation? Mech. Dev. *87*, 57–66.

Gelbke, H. (1951). The influence of pressure and tension on growing bone in experiments with animals. J. Bone Joint Surg. Am. *33-A*, 947–954.

Germiller, J.A., and Goldstein, S.A. (1997). Structure and function of embryonic growth plate in the absence of functioning skeletal muscle. J. Orthop. Res. *15*, 362–370.

Gerstenfeld, L.C., Cullinane, D.M., Barnes, G.L., Graves, D.T., and Einhorn, T.A. (2003). Fracture healing as a post-natal developmental process: molecular, spatial, and temporal aspects of its regulation. J. Cell. Biochem. *88*, 873–884.

Giannoudis, P.V., Einhorn, T.A., and Marsh, D. (2007). Fracture healing: the diamond concept. Injury *38* (*Suppl 4*), S3–S6.

Hall, B.K., and Herring, S.W. (1990). Paralysis and growth of the musculoskeletal system in the embryonic chick. J. Morphol. *206*, 45–56.

Huang, W., Foster, J.A., and Rogachefsky, A.S. (2000). Pharmacology of botulinum toxin. J. Am. Acad. Dermatol. *43*, 249–259.

Hunter, J. (1837). Of the diseases of bones and joints, of fractures, dislocations &c. In The Works of John Hunter, F.R.S. with Notes, *Vol. 1*, J.F. Palmer, ed. (London: Longman, Rees, Orme, Brown, Green, and Longman), pp. 498–535.

Husain, S.N., King, E.C., Young, J.L., and Sarwark, J.F. (2008). Remodeling of birth fractures of the humeral diaphysis. J. Pediatric Orthopaed. *28*, 10–13.

Kahn, J., Shwartz, Y., Blitz, E., Krief, S., Sharir, A., Breitel, D.A., Rattenbach, R., Relaix, F., Maire, P., Rountree, R.B., et al. (2009). Muscle contraction is necessary to maintain joint progenitor cell fate. Dev. Cell *16*, 734–743.

Karaharju, E.O., Ryöppy, S.A., and Mäkinen, R.J. (1976). Remodelling by asymmetrical epiphysial growth. An experimental study in dogs. J. Bone Joint Surg. Br. *58*, 122–126.

Karsenty, G., and Wagner, E.F. (2002). Reaching a genetic and molecular understanding of skeletal development. Dev. Cell *2*, 389–406.

Kronenberg, H.M. (2003). Developmental regulation of the growth plate. Nature *423*, 332–336.

Le, A.X., Miclau, T., Hu, D., and Helms, J.A. (2001). Molecular aspects of healing in stabilized and non-stabilized fractures. J. Orthop. Res. *19*, 78–84.

Murray, D.W., Wilson-MacDonald, J., Morscher, E., Rahn, B.A., and Käslin, M. (1996). Bone growth and remodelling after fracture. J. Bone Joint Surg. Br. *78*, 42–50.

Murtaugh, L.C., Chyung, J.H., and Lassar, A.B. (1999). Sonic hedgehog promotes somitic chondrogenesis by altering the cellular response to BMP signaling. Genes Dev. *13*, 225–237.

Nowlan, N.C., Murphy, P., and Prendergast, P.J. (2008). A dynamic pattern of mechanical stimulation promotes ossification in avian embryonic long bones. J. Biomech. *41*, 249–258.

Olsen, B.R., Reginato, A.M., and Wang, W. (2000). Bone development. Annu. Rev. Cell Dev. Biol. *16*, 191–220.

Riddle, R.D., Johnson, R.L., Laufer, E., and Tabin, C. (1993). Sonic hedgehog mediates the polarizing activity of the ZPA. Cell *75*, 1401–1416.

Roberts, G.J., and Blackwood, H.J. (1983). Growth of the cartilages of the midline cranial base: a radiographic and histological study. J. Anat. *136*, 307–320.

Sarmiento, A., Kinman, P.B., Galvin, E.G., Schmitt, R.H., and Phillips, J.G. (1977). Functional bracing of fractures of the shaft of the humerus. J. Bone Joint Surg. Am. *59*, 596–601.

Schindeler, A., McDonald, M.M., Bokko, P., and Little, D.G. (2008). Bone remodeling during fracture repair: the cellular picture. Semin. Cell. Dev. Biol. *19*, 459–466.

Schultz, A.H. (1939). Notes on Diseases and Healed Fractures of Wild Apes: And Their Bearing on the Antiquity of Pathological Conditions in Man. (Baltimore: Johns Hopkins University Press).

Schultz, A.H. (1944). Age changes and variability in gibbons. A Morphological study on a population sample of a man-like ape. Am. J. Phys. Anthropol. *2*, 1–129.

Shapiro, F. (2008). Bone development and its relation to fracture repair. The role of mesenchymal osteoblasts and surface osteoblasts. Eur. Cell. Mater. *15*, 53–76.

Sharir, A., Stern, T., Rot, C., Shahar, R., and Zelzer, E. (2011). Muscle force regulates bone shaping for optimal load-bearing capacity during embryogenesis. Development *138*, 3247–3259.

Shwartz, Y., Farkas, Z., Stern, T., Aszódi, A., and Zelzer, E. (2012). Muscle contraction controls skeletal morphogenesis through regulation of chondrocyte convergent extension. Dev. Biol. *370*, 154–163.

Shwartz, Y., Blitz, E., and Zelzer, E. (2013). One load to rule them all: mechanical control of the musculoskeletal system in development and aging. Differentiation *86*, 104–111.

Sijbrandij, S. (1963). Inhibition of tibial growth by means of compression of its proximal epiphysial disc in the rabbit. Acta Anat. (Basel) *55*, 278–285.

Strobino, L.J., Colonna, P.C., Brodey, R.S., and Leinbach, T. (1956). The effect of compression on the growth of epiphyseal bone. Surg. Gynecol. Obstet. *103*, 85–93.

Tencer, A.F. (2010). Biomechanics of fracture and fracture fixation. In Rockwood and Green's fractures in adults, C.A. Rockwood, D.P. Green, and R.W. Bucholz, eds. (Philadelphia: Lippincott Williams & Wilkins), pp. 3–38.

Thomopoulos, S., Kim, H.M., Rothermich, S.Y., Biederstadt, C., Das, R., and Galatz, L.M. (2007). Decreased muscle loading delays maturation of the tendon enthesis during postnatal development. J. Orthop. Res. *25*, 1154–1163.

Thompson, Z., Miclau, T., Hu, D., and Helms, J.A. (2002). A model for intramembranous ossification during fracture healing. J. Orthop. Res. *20*, 1091–1098.

Vortkamp, A., Pathi, S., Peretti, G.M., Caruso, E.M., Zaleske, D.J., and Tabin, C.J. (1998). Recapitulation of signals regulating embryonic bone formation during postnatal growth and in fracture repair. Mech. Dev. *71*, 65–76.

Wallace, M.E., and Hoffman, E.B. (1992). Remodelling of angular deformity after femoral shaft fractures in children. J. Bone Joint Surg. Br. *74*, 765–769.

Wilkins, K.E. (2005). Principles of fracture remodeling in children. Injury *36*, A3–A11.

Wilson-MacDonald, J., Houghton, G.R., Bradley, J., and Morscher, E. (1990). The relationship between periosteal division and compression or distraction of the growth plate. An experimental study in the rabbit. J. Bone Joint Surg. Br. *72*, 303–308.

Wolff, J. (1892). Das Gesetz der Transformation der Knochen. (Berlin: Quarto).

Young, B., Minugh-Purvis, N., Shimo, T., St-Jacques, B., Iwamoto, M., Enomoto-Iwamoto, M., Koyama, E., and Pacifici, M. (2006). Indian and sonic hedgehogs regulate synchondrosis growth plate and cranial base development and function. Dev. Biol. *299*, 272–282.

Developmental Cell, Volume *31*

Supplemental Information

A Mechanical Jack-like Mechanism Drives Spontaneous Fracture Healing in Neonatal Mice

Chagai Rot, Tomer Stern, Ronen Blecher, Ben Friesem, and Elazar Zelzer

Figure S1

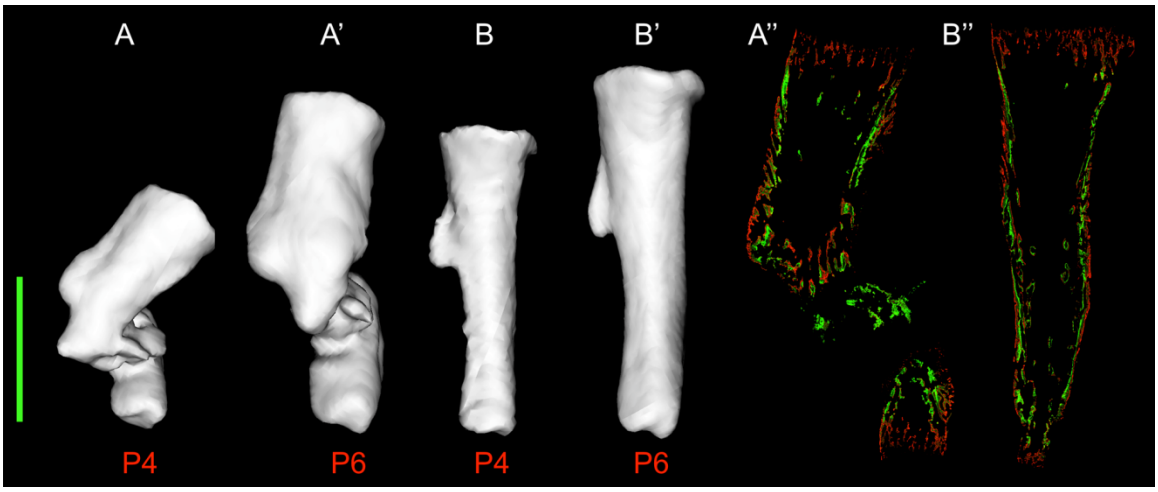

Figure S1. Natural reduction of fractured humeri is mediated by fragment movement (related to Figure 1). Fractured left humeri and corresponding intact right humeri were labeled at P3 with calcein (green) and scanned at P4 (A,B), then labeled at P5 with alizarin (red) and scanned at P6 (A',B'), followed by histological analysis (A'',B''). In both fractured and control bones calcein-labeled regions of the endosteum were maintained, negating the possibility of significant bone modeling. Scale bar: 2 mm.

Figure S2

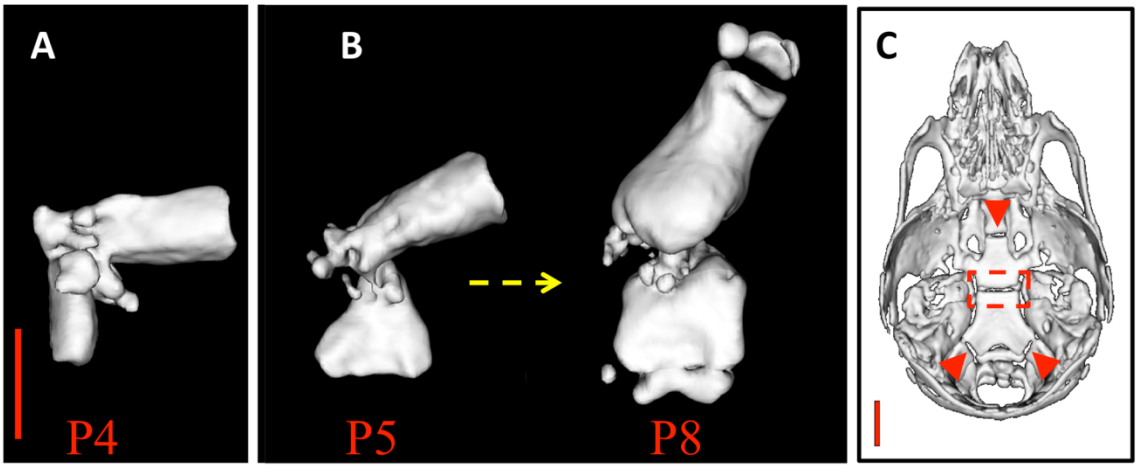

Figure S2. **CT images of humerus and skull base bones (related to Figure 3).** (A) µCT image showing a sagittal view of a severely angulated fractured humerus at P4. (B) µCT coronal views of a fractured humerus show that the bone undergoes substantial realignment between P5 and P8. (B) Bird's eye view µCT image of the skull base bones at P8. The sphenooccipital synchondrosis is demarcated by a rectangle and other synchondroses are indicated by red arrowheads. Scale bar: 2 mm.

Figure S3

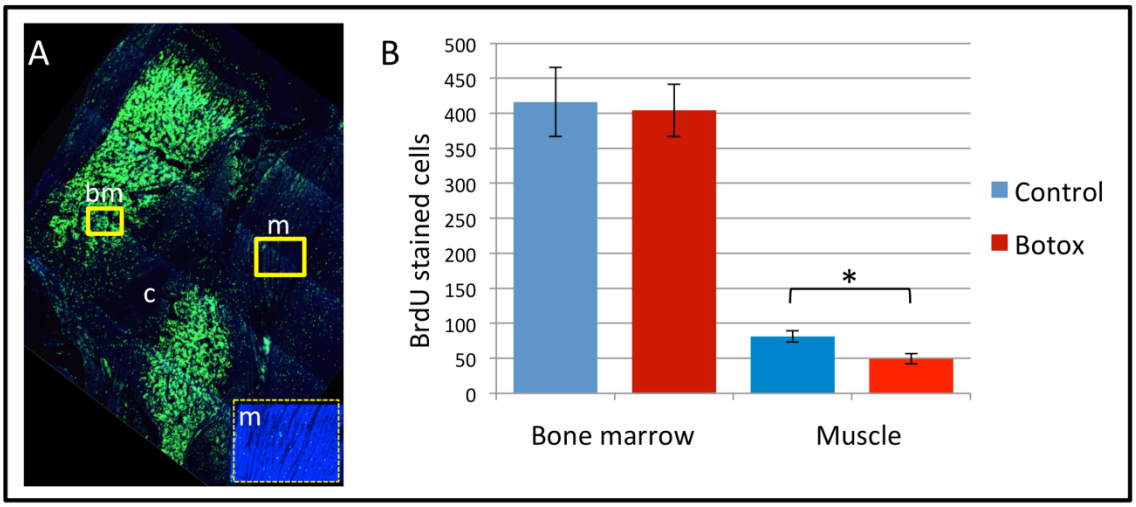

Figure S3. Cell proliferation in tissues surrounding the Botox injection site (related to Figure 6). (A) BrdU immunostaining of the fracture site of a P9 Botox-treated mouse. In the right lower corner is a magnification of the boxed area of muscle tissue. Abbreviations: c, callus; bm, bone marrow; m, muscle. **(B)** Comparison of cell proliferation (BrdU-positive cell count) in the boxed areas in A between Botox-injected and control mice. Proliferation of bone marrow cells was not affected by Botox treatment. In the muscle tissue, a small but statistically significant ($P \leq 0.05$, marked with an asterisk) reduction in proliferation was detected in Botox-treated mice. Data are represented as mean ± SEM.

Figure S4

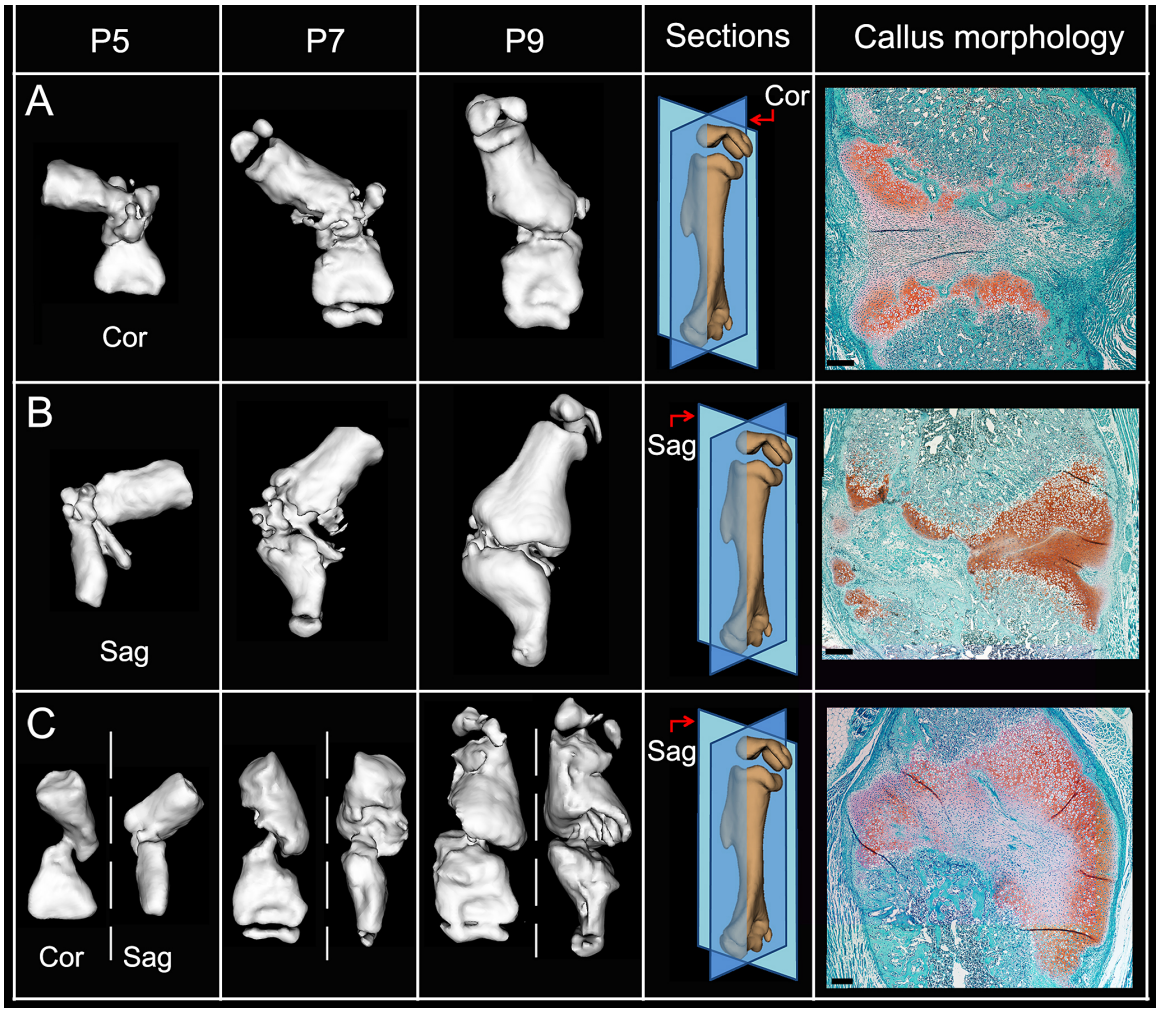

Figure S4. Morphological variation and complexity of fracture sites (related to Experimental Procedures, subsection "Animals and bone fracture induction"). (A,B) Simple fractures angulated mostly in the coronal (Cor) or sagittal (Sag) planes, respectively, during realignment from P5 to P9; section orientation is shown on the right. On the extreme right, Safranin O-stained sections indicate formation of a bidirectional growth plate at the concave side. **(C)** A complex fracture angulated in both planes is shown at P5 and during natural reduction until P9. Sagittal section demonstrates the more complex morphology of the fracture callus. Scale bars: 200 µm.

Supplemental Experimental Procedures

Bone fracture surgery

Humeral fractures were induced at postnatal day (P) 0. Mice were anesthetized by hypothermia and a lateral incision was made in the left limb near the mid-length of the bone. Using forceps, the triceps muscle was divided and the exposed bone was cut in the middle with small scissors. Then, the incision was closed with biological skin glue. Buprenorphine (2 mg/kg body weight) was used as analgesic, first during the procedure and then every 8-12 hours as needed. After surgery, mice were monitored daily by external examination and body weight was compared with control animals at the same age.

Ex vivo computed tomography (CT) analyses

To prepare samples for ex vivo CT analysis, harvested bones were fixed overnight in 4% paraformaldehyde (PFA/PBS) at 4ºC. Then, tissues were rinsed three times in PBS and stored at 4°C until scanning. Samples were scanned using a microfocussed X-ray tomographic system (Micro XCT-400, Xradia) at 40 kV and 200 lA. One thousand projection images were taken at a total integration time of 5 ms, with a linear magnification of X2 and a final pixel size of 5 μm. The volume was reconstructed using a back projection filtered algorithm (XRadia). 2D and 3D image data processing and analysis were carried out using MicroView software.

Preparation of histological sections

For all section analyses, limbs were fixed overnight in 4% PFA-PBS and decalcified at

4ºC in 19% EDTA (pH 7.4) for 7–14 days, depending on the mouse age. Then, tissues were dehydrated to 100% ethanol, embedded in paraffin and sectioned at a thickness of 7 μm.

Evaluation of bone deposition and resorption

Bone deposition and resorption were assessed by intraperitoneal injections of calcein (Sigma # C0875; 2.5 mg/kg body weight) into P3 or P6 mice and alizarin complexone (Sigma # a3882; 7.5 mg/kg) at P5 or P8. Limbs were harvested 24 hours after the second injection, fixed overnight in 4% PFA-PBS and dehydrated to 100% ethanol. Tissues were then embedded in JB-4 plastic resin (JB-4 Embedding Kit, Electron Microscopy Sciences, 14270–00) according to the manufacturer's protocol and sectioned at a thickness of 5 μm. Fluorescence was visualized using LSM510 laser-scanning confocal microscope (Carl Zeiss, Jena, Germany).

Bone registration and appositional growth calculations

Registration of micro-CT images was done manually using the free and open source software package 3D Slicer v. 3.6 (Pieper et al., 2006). To calculate appositional growth between consecutive developmental stages, external surfaces of both images were first isolated based on isosurface corresponding to Hounsfield value of 1500. Next, for each vertex on the surface of the later-stage bone, the closest vertex on the surface of the younger bone was found. Then, the absolute distance between the two vertices was calculated and the obtained value was color-coded using MATLAB software version R2013a (MathWorks Inc., Natick, MA).

Measurement of fracture angulation

To measure the angle between fracture fragments, the isosurface corresponding to Hounsfield value of 1500 was first extracted, thus generating a 3D representation of the ossified bone. Next, the formed surface was manually repositioned such that the distal fragment of the bone was placed vertically, i.e. in parallel to the *z*-axis of the image grid. The bone was further rotated about the vertical axis such that the formed (x,z) and (y,z) planes of the image grid would correspond with the sagittal and coronal anatomical planes. Then, the orthogonal projections of the isosurface on both sagittal and coronal planes were calculated and the angle between proximal and distal fragments was measured manually in each plane. Lastly, the fracture angle was calculated based on the measured angles using the following equation:

$$\alpha_{Fracture} = \tan^{-1}\left(\sqrt{\tan^2(\alpha_{Sagittal}) + \tan^2(\alpha_{Coronal})}\right)$$

Supplemental References

Pieper, S., Lorensen, B., Schroeder, W., and Kikinis, R. (2006). The NA-MIC Kit: ITK, VTK, pipelines, grids and 3D slicer as an open platform for the medical image computing community. Paper presented at: Biomedical Imaging: Nano to Macro, 2006 3rd IEEE International Symposium on (IEEE).